Ocean Systems Engineering, *Vol. 4, No. 2 (2014) 099-115*
DOI: http://dx.doi.org/10.12989/ose.2014.4.2.099

Safety assessment of caisson transport on a floating dock by frequency- and time-domain calculations

H.Y. Kang[a] and M.H. Kim[*]

Ocean Engineering Program, Department of Civil Engineering, Texas A&M University, 3136 TAMU, College Station, TX, USA, 77843-3136

(Received January 9, 2014, Revised April 25, 2014, Accepted May 28, 2014)

Abstract. When caissons are mounted on a floating transportation barge and towed by a tug boat in waves, motion of the floating dock creates inertia and gravity-induced slip forces on the caisson. If its magnitude exceeds the corresponding friction force between the two surfaces, a slip may occur, which can lead to an unwanted accident. In oblique waves, both pitch and roll motions occur simultaneously and their coupling effects for slip and friction forces become more complicated. With the presence of strong winds, the slip force can appreciably be increased to make the situation worse. In this regard, the safety of the transportation process of a caisson mounted on a floating dock for various wind-wave conditions is investigated. The analysis is done by both frequency-domain approach and time-domain approach, and their differences as well as pros and cons are discussed. It is seen that the time-domain approach is more direct and accurate and can include nonlinear contributions as well as viscous effects, which are typically neglected in the linear frequency-domain approach.

Keywords: caisson transport; floating barge; safety; slip force; friction force; inertia/gravity effects; nonlinear terms; roll-pitch coupling; frequency-domain and time-domain analysis; irregular waves/winds. initial inclination; deck flooding

1. Introduction

Caissons are used for various offshore and coastal structures. In particular, box-type caissons are popular as base unit for harbor walls and breakwaters. They can be built on land, inside dry-docks, or on floating barges and are typically transported to the installation site by floating transportation barges and tug boats.

When caissons are mounted on a floating transportation barge and towed by a tug boat in waves, motion of the floating dock creates inertia loading on the caisson. In addition, the inclination of the floating dock generates gravity-induced slip forces. The inertia and gravity-slip forces are resisted by the friction force at interface between the surfaces of floating-dock and caisson in the absence of any blockage or supporting lines. As sea environments get severer, the motions are increased, and the resulting slip force may exceed the resisting friction force. In this case, the slip and collision may occur between the caisson and blocking side walls of the floating dock. In oblique

*Corresponding author, Professor, E-mail: m-kim3@neo.tamu.edu
[a] E-mail: ga0prodg@neo.tamu.edu

 ISSN: 2093-6702 (Print), 2093-677X (Online)

waves, both pitch and roll motions occur simultaneously and their coupling effects for separating slips force and resisting friction forces become more complicated. With the presence of strong winds, the separation forces can significantly be increased to make the situation worse. Moreover, in the wet condition, the friction force can also be significantly reduced. In this regard, we investigate in this paper the safety of the transportation process of a caisson mounted on a floating dock for various wind-wave conditions. This is to figure out whether the transportation process is safe or not under the given system and environmental conditions (e.g., Kang *et al*. 2011).

The analysis can be done by either frequency-domain approach or time-domain approach. In the frequency-domain analysis, it is difficult to include nonlinear wave contributions, higher-order terms in equations of motions, and nonlinear viscous drag forces. In time-domain approach, they can be more straight-forwardly included. In both frequency- and time-domain approaches, there exist phase differences between the wind force, 6DOF inertia loadings, pitch-roll gravity-slip forces, and friction forces. Therefore, special attention needs to be paid to find the actual instantaneously maximum separation and minimum friction forces. In Seok *et al*. (2010), the frequency-domain analysis was based on displacement-velocity-acceleration RAOs, and thus phase effects were not accurately considered, which leads to more conservative predictions. In this paper, however, all the phase information between motion displacements, velocities, and accelerations are exactly taken into consideration so that the frequency-domain results for the separation and friction forces exactly coincide with the time-domain results when only linear wave exciting forces are applied. A similar analysis procedure can also be used for the design of buildings on floating islands or top-side tie-down structures and equipments of floating drilling and production platforms (Yang *et al*. 2010, 2011).

In the frequency-domain analysis, a 3D diffraction/radiation panel program (Lee *et al*. 1991) based on BIEM (Boundary Integral Equation Method) and linear potential theory was used. In the time-domain simulation, a hull-mooring coupled dynamic analysis program including viscous effects and various nonlinear contributions was used. The time-domain multi-vessel-mooring-riser coupled dynamic analysis program, HARP/CHARM3D, has been developed by the research group of the second author during the past decade (Ran 2000, Kim *et al*. 2001, Tahar and Kim 2003, Kim *et al*. 2005, Koo and Kim 2005, Kang and Kim 2012). The developed analysis/simulation methodology is used here for the safety assessment of the towing operation of barge-mounted caissons for any given sea environments.

2. General theory

To check the stability of a caisson on the floating dock, a set of equations are derived and used to get the friction and slip forces of the caisson. Both inertia and gravity forces act simultaneously and contribute to the friction and slip forces of the caisson. Two coordinate systems (global and body-fixed coordinates) are introduced and all the dynamic relations are expressed with respect to the floating-dock-fixed coordinate system. The derivations of the inertia and gravity forces are presented below. Using the derived equations by substituting floating body's kinematics, slip and friction forces can be investigated in both frequency and time domains. The floater's kinematic information is achieved by solving wave-floater interactions based on the potential theory and Cummins Equation. In time domain, irregular waves are applied to the caisson on a floating dock towed by a vessel. The towing hawser lines are realized by the coupled nonlinear mooring line dynamics (Ran 2000).

2.1 Intertia force

Two coordinate systems with origins *O* and *B* are shown in Fig. 1. The first frame *O* represents global coordinate system and the second one *B* represents the body-fixed coordinate system. The frame *B* is attached to the floating dock, and a point of interest *P* is assumed to be the center of gravity of the caisson.

To define the acceleration of the point *P*, both translational- and rotational-motion-induced accelerations need to be considered and they can be combined together as follows

$$a_P = a_B + \alpha \times r_{P/B} + \omega \times (\omega \times r_{P/B}) \tag{1}$$

The first term a_B is the translational acceleration of the floating dock and the next term $\alpha \times r_{P/B}$ is the tangential acceleration of the caisson due to the rotational acceleration α of the floating dock. The last term $\omega \times (\omega \times r_{P/B})$, in which ω is angular velocity, is the centripetal acceleration of the caisson. Then, a 3-dimensional matrix of the inertia force can be derived by the acceleration multiplied by a mass matrix of the caisson.

$$\begin{aligned} F_{inertia} = \begin{bmatrix} m & 0 & 0 \\ 0 & m & 0 \\ 0 & 0 & m \end{bmatrix} \Bigg(& \begin{Bmatrix} \ddot{x} \\ \ddot{y} \\ \ddot{z} \end{Bmatrix} - \begin{bmatrix} 0 & -r_z & r_y \\ r_z & 0 & -r_x \\ -r_y & r_x & 0 \end{bmatrix} \begin{Bmatrix} \ddot{\theta}_x \\ \ddot{\theta}_y \\ \ddot{\theta}_z \end{Bmatrix} \\ & - \begin{bmatrix} 0 & -\dot{\theta}_z & \dot{\theta}_y \\ \dot{\theta}_z & 0 & -\dot{\theta}_x \\ -\dot{\theta}_y & \dot{\theta}_x & 0 \end{bmatrix} \begin{bmatrix} 0 & -r_z & r_y \\ r_z & 0 & -r_x \\ -r_y & r_x & 0 \end{bmatrix} \begin{Bmatrix} \dot{\theta}_x \\ \dot{\theta}_y \\ \dot{\theta}_z \end{Bmatrix} \Bigg) \end{aligned} \tag{2}$$

Since the above inertia force is expressed in global coordinate system, proper transformation is necessary to express the force with respect to the body-fixed coordinate system if the floating dock has instantaneous trim, heel, or yaw angles. The Euler 3-2-1 coordinate-transform sequence is adopted to find the component of each force with respect to the body-fixed coordinate system in three-dimensional space.

$$E = \begin{bmatrix} 1 & 0 & 0 \\ 0 & \cos\theta_x & \sin\theta_x \\ 0 & -\sin\theta_x & \cos\theta_x \end{bmatrix} \begin{bmatrix} \cos\theta_y & 0 & -\sin\theta_y \\ 0 & 1 & 0 \\ \sin\theta_y & 0 & \cos\theta_y \end{bmatrix} \begin{bmatrix} \cos\theta_z & \sin\theta_z & 0 \\ -\sin\theta_z & \cos\theta_z & 0 \\ 0 & 0 & 1 \end{bmatrix} \tag{3}$$

The final form of the inertia force in the body-fixed coordinate system can then be expressed as

$$F_{inertia}^{B} = E \cdot F_{inertia} \tag{4}$$

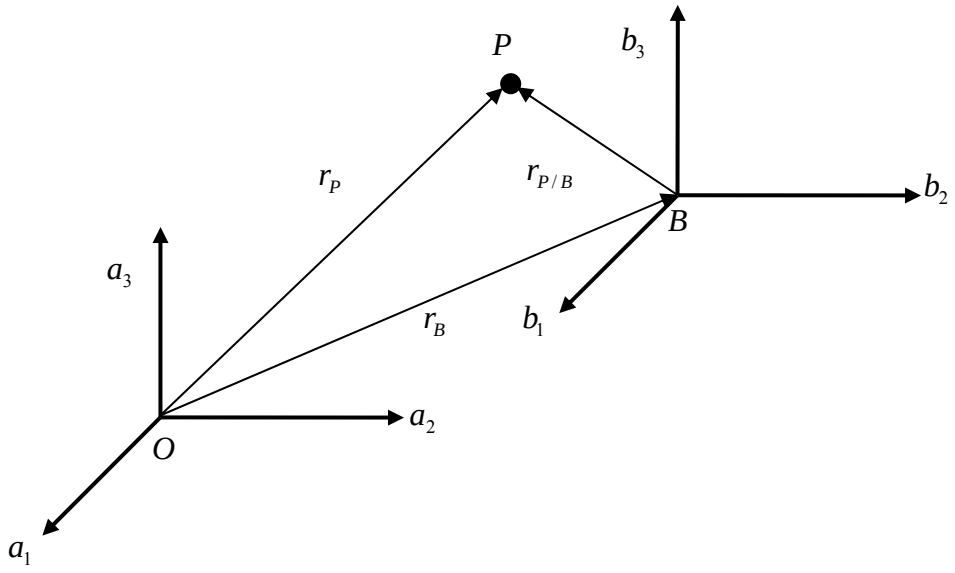

Fig. 1 Earth-fixed and body-fixed coordinate systems

2.2 Gravity force

In case of static-equilibrium condition, only the vertical component of the gravity force needs to be considered. However, with continuous translational and rotational motions of the floating dock, additional components are produced from gravity force of the caisson with respect to the body-fixed coordinate system. The instantaneous gravity-induced slip force in the body-fixed coordinate system can be derived by using the transformation matrix E as follows

$$F_{gravity}^{B} = E \begin{bmatrix} 0 \\ 0 \\ -mg \end{bmatrix} \tag{5}$$

2.3 Nonlinear friction and slip forces

Using the full equations including Euler angles, time-domain simulations can be performed including nonlinear contributions not only for nonlinearities of wave effects but also for higher-order terms in the full equations above.

$$F_{slip} = \sqrt{\left(F_{slip}^{x}\right)^2 + \left(F_{slip}^{y}\right)^2}, \text{ where } F_{slip}^{x,y} = -F_{inertia}^{Bx,y} + F_{gravity}^{Bx,y} \tag{6}$$

$$F_{friction} = \mu\left(F_{inertia}^{Bz} - F_{gravity}^{Bz}\right) \tag{7}$$

The first term in the right-hand side of (7) consists of contributions from heave acceleration, rotational acceleration, and centripetal acceleration i.e., the z components of (4). The inertial contributions become more important in resonance or high-frequency regions.

Prior to the time domain analysis, linearized analysis in the frequency domain is conducted first and the results are compared with the corresponding time-domain results.

2.4 Linearized friction and slip forces for frequency-domain analysis

If rotation angles are very small, we can linearize the friction and slip forces by setting $\cos\theta \approx 1$, $\sin\theta \approx \theta$ and eliminating all the second-order terms. In this study, r_x terms can be eliminated additionally since $r^{P/B} = (0, r_y, r_z)$.

$$F_{slip}^{x} = -F_{inertia}^{x} + F_{gravity}^{x} = -m\left(\ddot{x} + r_z\ddot{\theta}_y - r_y\ddot{\theta}_z - g\theta_y\right) \tag{8}$$

$$F_{slip}^{y} = -F_{inertia}^{y} + F_{gravity}^{y} = -m\left(\ddot{y} - r_z\ddot{\theta}_x + r_x\ddot{\theta}_z + g\theta_x\right) \tag{9}$$

$$F_{friction} = \mu(F_{inertia}^{z} - F_{gravity}^{z}) = \mu m\left(g + \ddot{z} + r_y\ddot{\theta}_x + r_x\ddot{\theta}_y\right) \tag{10}$$

In frequency domain, there are two ways to obtain the friction and slip forces. One is the direct use of motion RAO's (complex variable including phase) by substitution into Eqs. (8)-(10) and obtain slip and friction forces for respective incident wave periods. The other is an approximate method for which the respective contributions in Eqs. (8)-(10) are added without considering phase effect (e.g., Seok *et al*. 2010). Of course, this approximate approach is simpler and will lead to more conservative results. We note that each force term is associated with the response including phase, so the phase differences between respective motions should be considered if accurate estimation of slip/friction-force RAOs is to be made.

In case of irregular waves, the corresponding friction/slip-force RAOs can be used to calculate the respective force spectra. The formula is given by

$$S_f(\omega) = \left|H(\omega)\right|^2 S_w(\omega) \tag{11}$$

where $S_f(\omega)$, $S_w(\omega)$ represent the responding force spectrum and incident wave spectrum respectively, and $H(\omega)$ represent the slip or friction force RAO. For a linear system, if the input wave is Gaussian random process, the output responding spectrum also follows the Gaussian random process. The area under the force spectrum m_0 represents their variance, and the most probable maximum value $F_{\max}$ is given by

$$F_{\max} = \sqrt{2m_0 \ln\frac{t}{T_2}} \tag{12}$$

where t is the time duration, T_2 is the mean wave period defined as $T_2 = 2\pi\sqrt{m_0/m_2}$, and m_n is nth spectral moment.

3. Case study

In the present study, we consider a floating dock with a caisson a little asymmetrically (1.8 m off from center) placed, as shown in Fig. 2. For the purpose of numerical analysis, the towing effect is altered by head-current effect with the same speed, 1 m/sec. And the friction coefficient μ is assumed to be 0.4, which is a typical value between dry dock and caisson surfaces. In a very wet condition, the friction coefficient can be significantly lowered, and thus special caution is needed.

3.1 Particulars of floating dock and environmental condition

The particulars of the floating dock including the caisson are given in Table 1. A potential-theory-based 3D diffraction/radiation panel program (Lee *et al*. 1991) is used to obtain hydrodynamic coefficients and wave forces on the floating dock. The wetted surface of the system is modeled by 704 panels as shown in Fig. 3. After obtaining all the hydrodynamic coefficients from the 3D diffraction/radiation program, they are used in the subsequent time-domain simulations. In the time-domain simulations, longitudinal and transverse vertical plates of equivalent projected areas are also modeled to capture the hull-viscous-damping effects by the combined effects of waves and currents.

Fig. 2 Schematic view of transferring a caisson on a floating dock

Table 1 Particulars of floating dock with caisson and ballast included

Displacement	20,598 ton	Caisson/Ballast	10,700/3,812.105 ton
Length	72.0 m	KG	10.14 m
Breadth	47.2 m	Kxx/Kyy/Kzz	14.69/19.67/21.51 m
Side wall height / Draft / Freeboard	19 / 6.0 / 0.4 m	Kxy/Kyz/Kzx	-0.65/1.92/-0.07 m

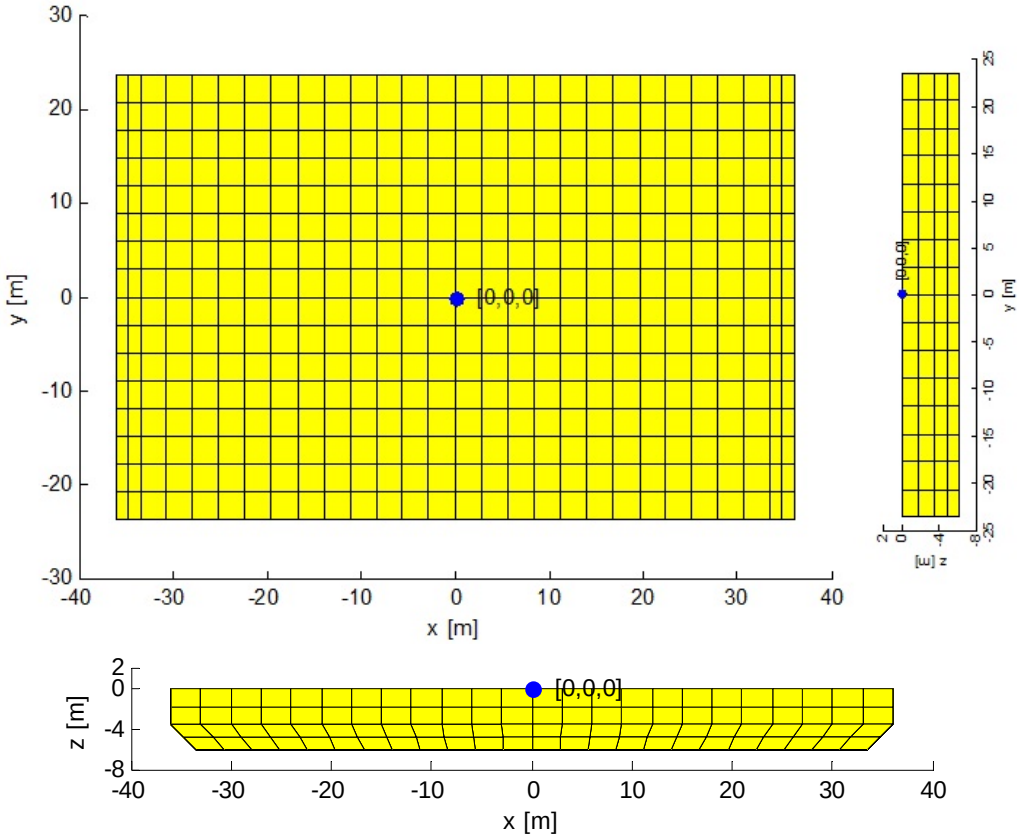

Fig. 3 Paneled model of the wetted surface of the floating dock

The applied sea states are given in Table 2, based on WMO (World Meteorological Organization) code. To generate incident waves, two-parameter P-M (Pierson-Moskowitz) wave spectrum is used, as shown in Fig. 4. Fig. 4(a) shows that the generated wave spectra agree very well with the given theoretical input spectra. The wave headings are defined from the positive longitudinal-x-axis along counter-clock wise; 3 wave headings, 0˚, 45˚, and 90˚, are used. The water depth is 30 m. To simulate time-varying wind velocities, three different API wind spectra corresponding to each sea state are used, as shown in Fig. 4(b). It is seen that the dynamic wind may strongly influence low-frequency slowly-varying responses.

Table 2 Environmental conditions

Sea State	Significant Wave Height	Peak Period	Sustained Wind Speed
3	0.88 m	7.8 sec	6.95 m/sec
4	1.88 m	8.8 sec	9.77 m/sec
5	3.25 m	9.7 sec	12.6 m/sec

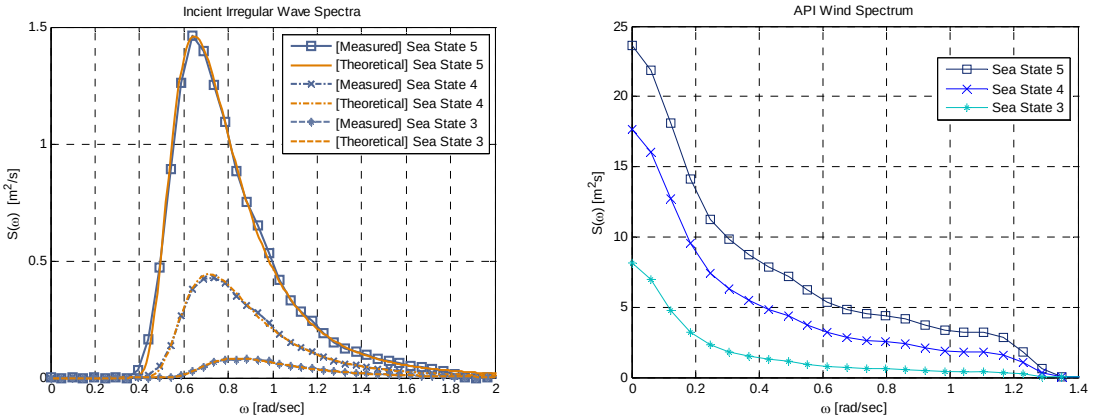

Fig. 4 Spectral comparisons of irregular waves and winds

3.2 Numerical simulation results

For the present system, the global-coordinate origin is located on the mean water level. The heave, roll and pitch RAO's of the floating dock with the caisson are plotted in Fig. 5 for three wave headings, 0˚, 45˚, and 90˚. Both heave and roll have the largest values in beam (90˚) waves. The frequency-domain results are also compared with the time-domain results for two different sea states, 3 and 5. The time-domain RAOs are calculated by using Eq. (11) after generating response time series. In the frequency-domain calculations, the RAO values are obtained for each regular wave frequency ω, but in the time-domain simulations, all the RAO values are simultaneously obtained from Eq. (11). If the system is linear, the RAOs should remain the same regardless of the incident wave heights. However, in the time-domain simulations, several nonlinear effects exist, such as nonlinear hull viscous drag forces evaluated at instantaneous body positions, higher-order terms in the equation of motion in calculating slip and friction forces, and second-order mean and slowly-varying wave loads etc., therefore, the resulting RAOs may vary depending on incident-wave conditions. As can be seen in Fig. 5, when the sea state is milder, the results better agree with the linear frequency-domain results. At higher sea states, nonlinear contributions play more important role, which causes more deviation from the linear-potential result.

In case of oblique incidence angle, both roll and pitch motions occur and they cause slip forces in both directions. The maxima of the two rotational motions are not likely to occur at the same time. So, it is in general not clear when and in which direction the maximum friction and slip forces will occur. In the time-domain simulation, all the phase effects are automatically included. However in the frequency domain analysis, care must be taken to include all the phase effects accurately, as explained in the general theory part.

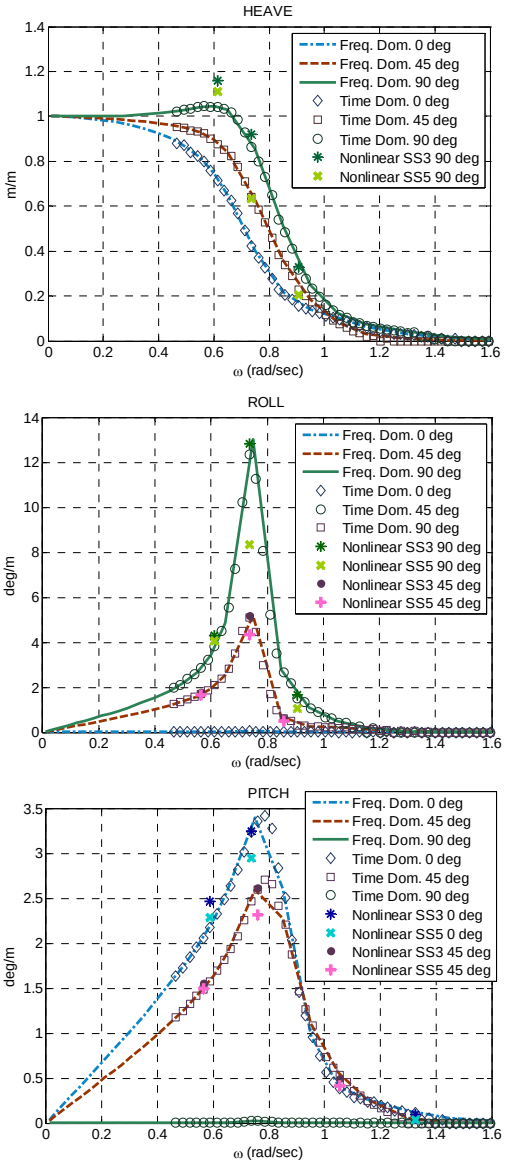

Fig. 5 Comparison of RAO's for 0˚, 45˚, and 90˚ wave headings (Sea State 5 for time domain)

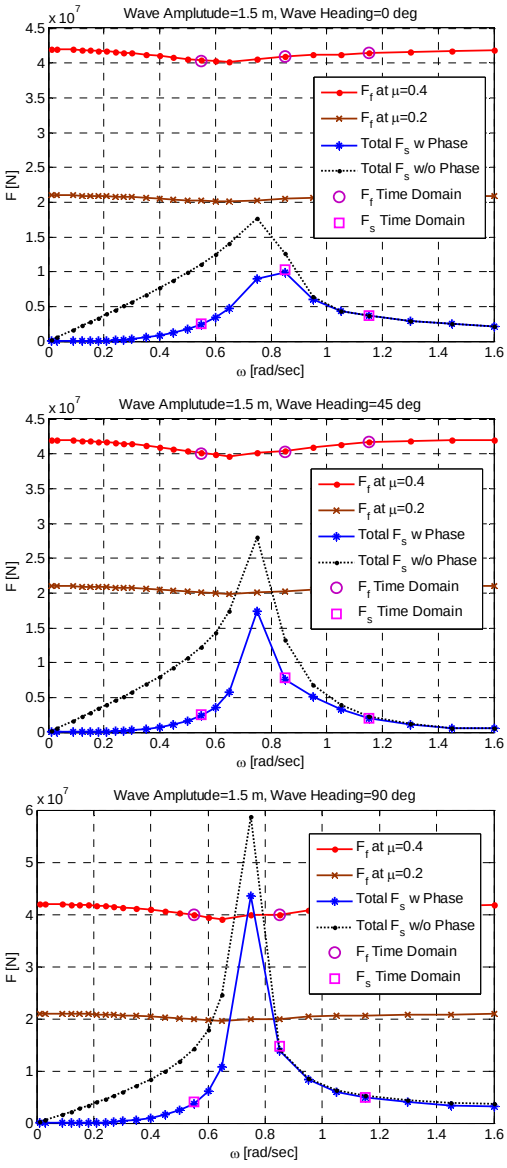

Fig. 6 Friction and slip forces as function of wave frequency

In case of a regular wave, if all the phases of the respective terms in the linear Eqs. (8)-(10) are correctly considered in the frequency-domain analysis, the resulting slip/friction forces should coincide with those of the time-domain simulation with the condition that all the nonlinear and viscous contributions are eliminated. The nonlinear terms in the equations of motions on time domain approach may still occur small discrepancy from frequency domain.

Fig. 6 shows that kind of agreement between the frequency- and time-domain analyses. The second one is the oblique-incidence case, so both roll and pitch motions are generated. From this comparison with excellent agreement, we can prove that the coupling effects between the roll and pitch motions are correctly captured in the frequency-domain analysis i.e., all the phase differences of (8)-(10) are correctly evaluated. The dotted line in the same figure is the corresponding slip force, for which the amplitudes of respective contributions are added without considering their phase differences (e.g., Seok *et al*. 2010). If only motion RAOs are available without phase information, this is the only way to obtain the corresponding slip-force RAO. Of course, this will lead to more conservative prediction, as shown in the figure, which can be regarded as a kind of safety factor. In case of the friction force, its value is dominated by the caisson weight, so almost invariant against wave frequencies. However, the z acceleration and centrifugal acceleration can slightly reduce the friction force when their effects are not negligible. From Fig. 6, it can be concluded that the beam wave condition with wave frequency near 0.75 rad/s is the worst case.

The regular-wave results from the exact frequency-domain analysis are given in Table 3. Results are obtained for 3 different wave heights equivalent to significant wave heights of sea states 3, 4 and 5, and three different wave headings. Peak frequencies for the slip force are 0.75 rad/s for quartering/beam waves and 0.85 rad/s for head waves. According to the table, in the case of a beam regular wave of about 3 m height, the slip force exceeds friction force and slip is likely to occur even for conservative dry-friction coefficient of 0.4. This result is based on the linear potential theory without including viscous effects, so the results are expected to be somewhat exaggerated since roll and pitch motions are to be reduced in time-domain simulations after including viscous hull damping. This will further be discussed in the next section.

Table 3 Comparison of friction force / slip force at peak frequency

Wave Height	Head Sea (0 deg)	Quartering Sea (45 deg)	Beam Sea (90 deg)
0.88 m	4.090E+7 N / 2.911E+6 N	4.142E+7 N / 5.083E+6 N	4.133E+7 N / 1.275E+7 N
1.88 m	4.090E+7 N / 6.219E+6 N	4.081E+7 N / 1.086E+7 N	4.063E+7 N / 2.724E+7 N
3.25 m	4.090E+7 N / 1.024E+7 N	3.998E+7 N / 1.877E+7 N	3.967E+7 N / 4.710E+7 N

3.3 Time-domain analysis for friction and slip forces

From the fact that this system is the most vulnerable to the beam wave condition in terms of the largest responses and slip forces, time-domain simulations are conducted for various irregular beam waves and their statistical results are compared with those given by spectral method in frequency domain based on (11) and (12). In the time-domain analysis, nonlinear forces, such as higher-order terms in the equations of motions, exact directional cosines, viscous drag and

damping, etc. are included. When necessary, the towing effect is also included through a head steady uniform current. Furthermore, the second-order slowly-varying wave drift forces and motions are included in the time-domain simulations by using Newman's approximation. Moreover, the cross-flow viscous effects on the hull are captured by using longitudinal/transverse equivalent drag-plates of the same projected areas through the use of Morison Equation. The drag coefficient is assumed to be 2 with the projected areas. 2 drag plates for surge direction and 3 drag plates for sway direction are used. In our previous studies, the present approach for hull viscous damping has been reasonably correlated against experimental measurement (e.g., Zhang *et al*. 2009, Kang *et al*. 2010).

At first, comparison between the spectral method and the direct reading from the time-domain analysis is given in Table 4 in terms of the maximum slip force and minimum friction force. For comparison purpose against frequency-domain results, only beam random waves are applied to the time-domain analysis i.e., no current and no wind for Table 4. It is seen that the frequency-domain spectral analysis generally underestimates the maximum slip force when compared against time-domain results. As for the minimum friction force, frequency-domain approach can either overestimate or underestimate compared to the time-domain results. In sea state 5, the difference between the minimum friction force and maximum slip force is 21 MN in frequency-domain case but it is 15.1 MN in time-domain case with the conservative dry-friction coefficient of 0.4.

Table 4 Comparison between spectral method and time-domain simulation

Sea State	Maximum Slip Force		Minimum Friction Force	
	Spectral Method	Time domain	Spectral Method	Time domain
3	4.88E+6 N	8.51E+6 N	3.77E+7 N	4.10E+7 N
4	1.12E+7 N	1.74E+7 N	4.09E+7 N	3.97E+7 N
5	1.90E+7 N	2.28E+7 N	4.00E+7 N	3.79E+7 N

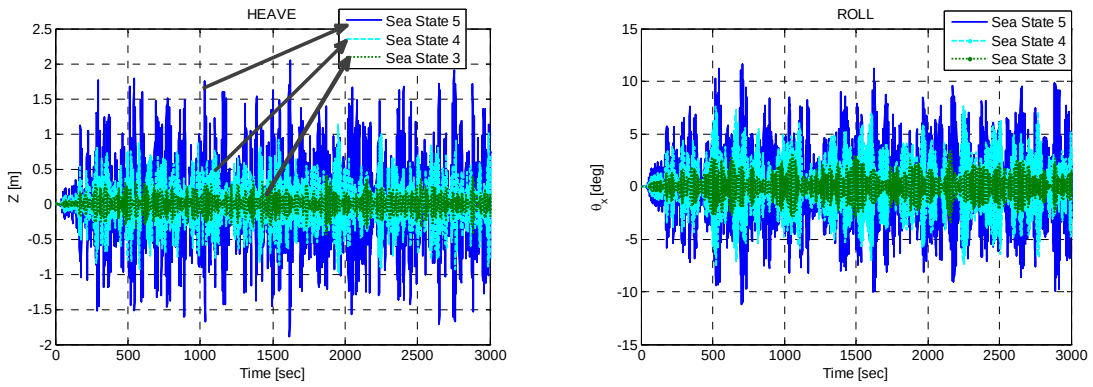

Fig. 7 Records of heave and roll for irregular beam wave applied

The time-domain results for Table 4 are shown in Figs. 7 and 8. Fig. 7 shows heave and roll motions of the floating barge. The motion amplitudes increase significantly in higher sea states. For the time-domain signals of slip forces, the negative values are converted to positive values to directly compare all the amplitudes regardless of their signs. From these figures, it is shown that the system is safe under irregular beam wave conditions even for sea state 5 as long as dry condition is met. However, if friction is reduced to half due to wet condition, failure may happen at the sea state 5, as shown in the figure. In the case of irregular waves with wind and towing speed, more reliable time-domain safety analysis needs to be used to identify the real failure conditions and take account into the design of the towing system and related operability.

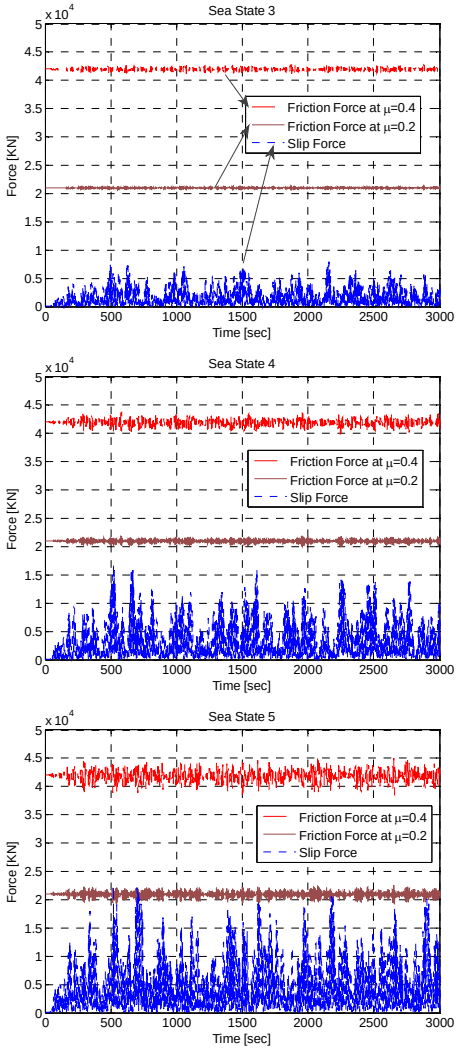

Fig. 8 Records of friction and slip forces for irregular beam wave only applied

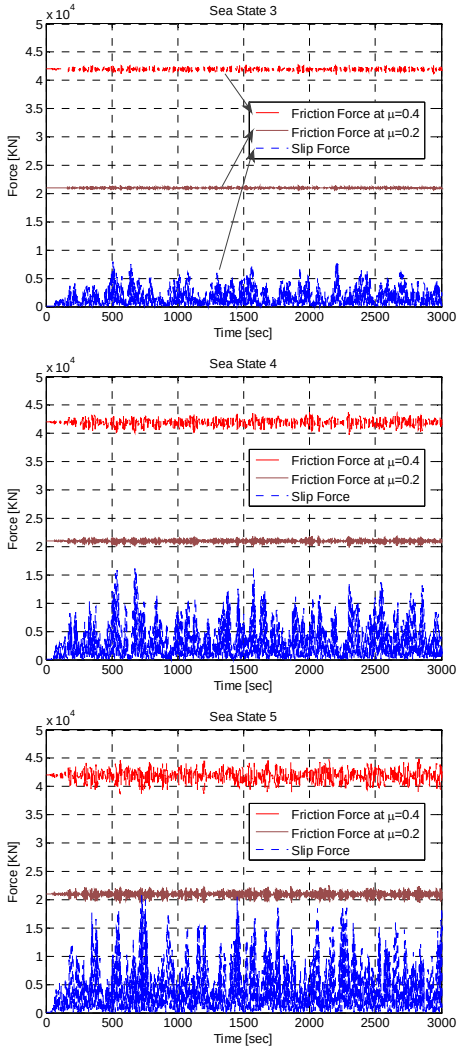

Fig. 9 Records of friction and slip forces for irregular beam wave, beam wind and head current applied

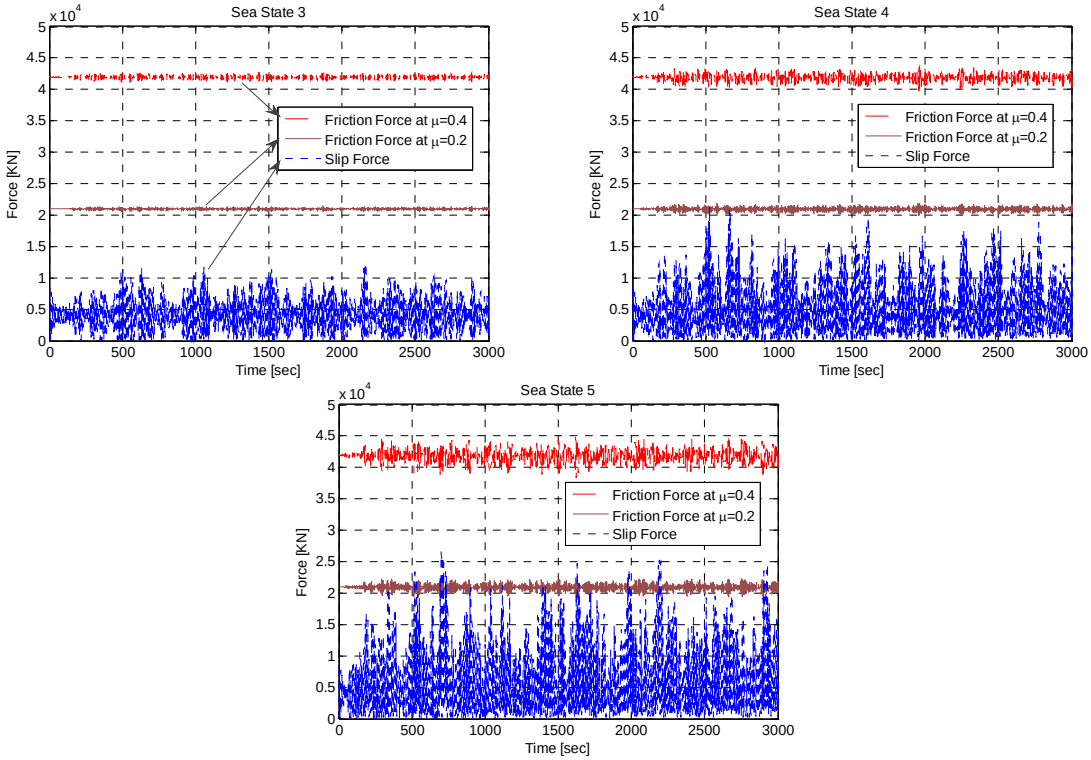

Fig. 10 Records of friction and slip forces for irregular beam wave applied with initial inclination

In this regard, in Fig. 9, we added the effects of beam winds and head currents in addition to the wave condition of Fig. 8. The floating dock is assumed to have side blocks, as shown in Fig. 2, and the wind loading is applied on it. However, there is shielding effect for the caisson behind the wall, and the wind loading on the caisson from the beam direction is only applied to the exposed projected area. In this non-collinear environmental condition, the maximum slip forces are about the same as those of Fig. 8. This means that the corresponding wind loading is relatively small compared to the roll stiffness or wave loading so that the increase of heel angle is almost negligible. It is also found that the effect of additional head current is not significant. The factor of safety for each sea state can be obtained from the ratio of minimum friction force to maximum slip force. However, it needs to be remarked that during wet condition, the friction coefficients used for dry conditions in Figs. 8 and 9 can be significantly reduced to expose the system to higher risk. It is particularly so with such a small freeboard of 0.4 m. This has to be additionally taken into consideration when determining the safety factor of the operation.

As mentioned earlier, the center of the caisson is not located at the center of the floating barge. Instead, it is 1.8 m off-center. It is due to the space for work and transportation while the caisson is constructed on the floating dock. Because of this misalignment, the barge is to be slightly tilted. So far, it is assumed that the floating barge is properly ballasted to have an even keel. If the barge was not properly ballasted in the absence of ballasting mechanism, there would be some small initial

inclination of the hull due to the misalignment of the caisson. So, the gravity-induced slip force may be increased in that direction. Due to the hull asymmetry, the mass and hydrostatic-coefficient matrices are also slightly changed. In the simulations of Fig. 10, those effects are considered and the results are compared against Fig. 8. We can see that slip forces are increased due to those additional considerations.

Fig. 11 shows the constituent components of friction forces. We can see in the top figure that the weight-induced friction forces are much bigger than vertical-acceleration-induced friction forces. The vertical-acceleration-induced friction force consists of three components (bottom figure), translational-acceleration-induced friction, rotational-acceleration-induced friction, and centripetal-acceleration-induced friction. It is seen that the heave-acceleration-induced friction is the most important among the inertial contributions.

Finally, Figs. 13 and 14 present relative wave elevations at four corners (see Fig. 12) of the floating barge. The relative wave elevations were calculated by the differences of disturbed (incident + diffracted + radiated) wave elevations and the positions of the reference points by barge motions. Since the relative wave elevations have been made with respect to the deck at z=0.4 m, the relative elevation over zero means flooding condition. Considering the configuration of the floating dock with side walls and beam wave direction, the flooding can occur mainly at open space (front and rear side with the width of 14.4 m) between the two side walls. Without side walls, the caisson is to be directly exposed to green waters (flooded water on deck) even at sea-state 3, and thus the free board of 0.4 m is not sufficient. In this regard, the oblique- or head-incidence case is more concerned with regard to the deck flooding in the absence of additional protective walls in that direction. If green water happens, the friction force is to be significantly decreased and water-contact forces may be added on the caisson. Therefore, even the sea state 3 may not be safe enough with the given free board.

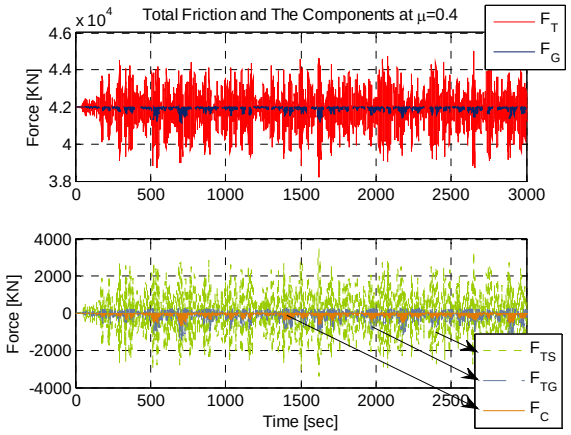

Fig. 11 Comparisons of constituent components of friction forces for sea state 5 case of Fig. 8 (F_T=total friction, F_G=weight-induced friction, F_{TS}=translational-acceleration-induced friction, F_{TG}=rotational-acceleration-induced friction, and F_C=centripetal-acceleration-induced friction)

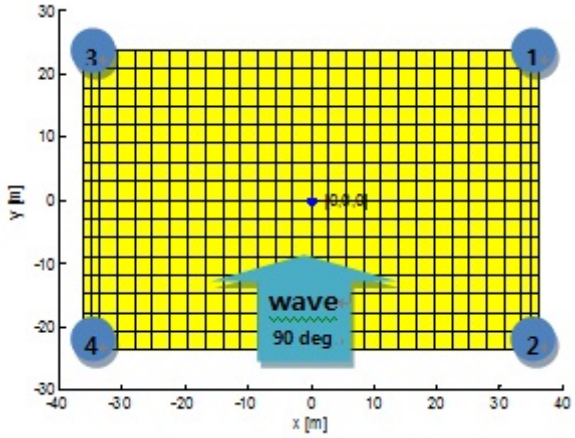

Fig. 12 Schematic view of reference points for relative wave elevation (four corners of floating barge top surface at z=0.4 m)

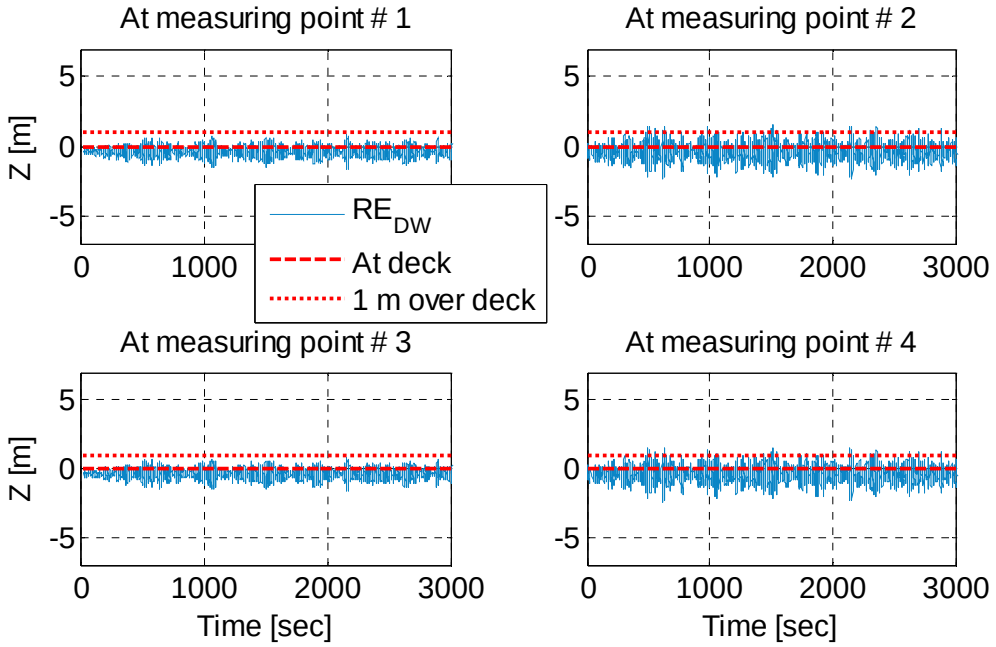

Fig. 13 Records of relative elevations at reference points with respect to the disturbed wave field for irregular-beam-wave-only case applied at sea state 3

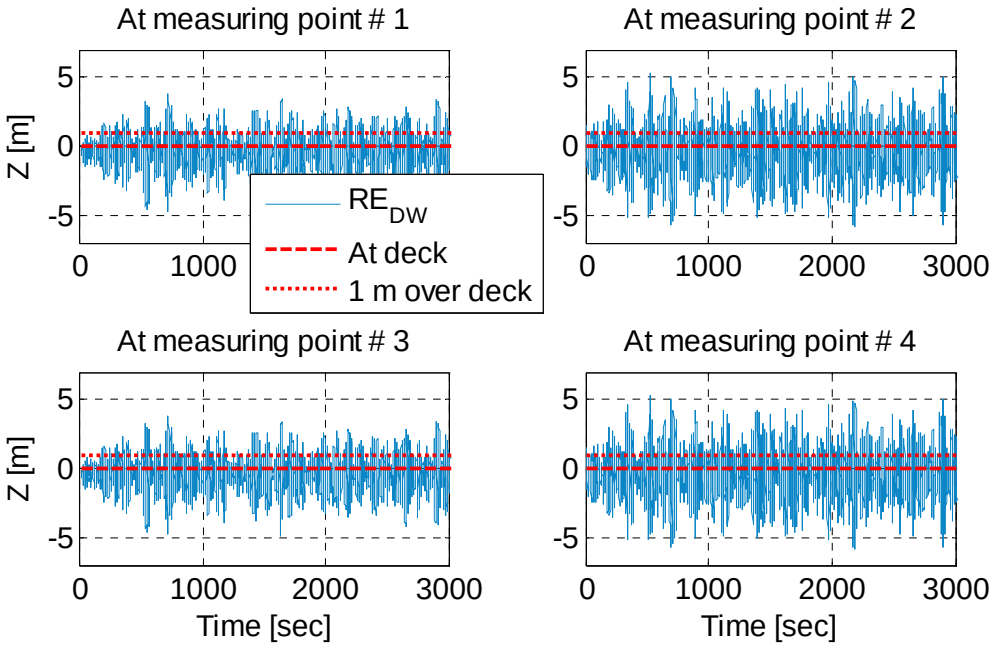

Fig. 14 Records of relative elevations at reference points with respect to the disturbed wave field for irregular-beam-wave-only case applied at sea state 5

5. Conclusions

The stability of a caisson on the deck of a floating barge can be evaluated in terms of friction and slip forces. For the evaluation, both frequency-domain and time-domain analyses can be used. In the frequency-domain approach, only linear terms are kept, so its procedure is simpler but the phase differences among various gravity and inertia terms need to be carefully taken into consideration. Whereas the time-domain approach is more direct and accurate and can include nonlinear contributions and viscous effects, which are typically neglected in the linear frequency-domain approach. The frequency-domain approach is still useful since it shows reasonable trend and gives at least the right order of magnitude. When the center lines of caisson-barge system are not properly aligned without proper ballasting, the initial inclination occurs and the system safety becomes worse due to the increased gravity-induced slip force. The effects of steady towing condition on overall system safety are not significant due to the fact that the slip force is mainly induced by dynamics and inclination of the floating dock.

In case of oblique incidence angle, both surge-sway and roll-pitch accelerations contribute to the maximum slip force and minimum friction force, and their coupling effects among various inertia and gravity terms can more straight-forwardly be treated in the time-domain simulations. The system is the most dangerous and unstable in beam waves and beam winds with upper deck wet, so this condition needs to be avoided. However, for the given configuration with side walls, deck flooding is more likely to happen in oblique and head waves and sufficient free board or additional protective walls need to be given with respect to the maximum operational sea state.

Acknowledgments

This study is financially supported by Samsung C&T Corporation and the financial support is gratefully appreciated.

References

Kang, H.Y., Kim, M.H., Kim, J.H., Park, W.S. and Chae, J.W. (2010), "On/offloading from both sides of a super container ship to land and floating harbor", *Proceedings of the 20th International Offshore and Polar Engineering Conference*, Peking, China.

Kang, H.Y., Kim, M.H., Seok, J., Park, J.C. and Kang, Y.K. (2011), "Safety of caisson transport on a floating dock", *Proceedings of the 21th International Offshore and Polar Engineering Conference*, Maui.

Kang, H.Y. and Kim, M.H. (2012), "Hydrodynamic interactions and coupled dynamics between a container ship and multiple mobile harbors", *Ocean Syst. Eng.*, **2**(3), 217-228.

Kim, M.H., Koo, B.J., Mercier, R.M. and Ward, E.G. (2005), "Vessel/mooring/riser coupled dynamic analysis of a turret-moored FPSO compared with OTRC experiment", *Ocean Eng.*, **32**, 1780-1802.

Kim, M.H., Ran, Z. and Zheng, W. (2001), "Hull/mooring coupled dynamic analysis of a truss spar in time domain", *Int. J. Offshore Polar*, **11**(1), 42-54.

Koo, B.J. and Kim, M.H. (2005), "Hydrodynamic interactions and relative motions of two floating platforms with mooring lines in side-by-side offloading operation", *Appl. Ocean Res.*, **27**(6), 295-310.

Lee, C.H., Newman, J.N., Kim, M.H. and Yue, D.K.P. (1991), "The computation of second-order wave loads", *Proceedings of the 10th International Offshore Mechanics and Arctic Engineering Conference*, Stavanger, Norway.

Ran, Z. (2000), *Coupled dynamic analysis of floating structures in waves and currents*, Ph.D. Dissertation, Texas A&M University, College Station, TX.

Seok, J., Park, J.C., Heo, J.K., Kang, H.Y., Bae, Y.H., Kim, M.H. and Kang, Y.K. (2010), "Stability evaluation during transportation of caisson for breakwater", *J. Ocean Eng. Technol.*, KSOE, **24**(4), 13-22.

Tahar, A. and Kim, M.H. (2003), "Hull/mooring/riser coupled dynamic analysis and sensitivity study of a tanker-based FPSO", *Appl. Ocean Res.*, **25**, 367-382.

Yang, C.K., Bae, Y.H., Kim, M.H. and Ward, E.G. (2010), "Loads on tie-down systems for floating drilling rigs during hurricane conditions", *Int. J. Offshore Polar*, ISOPE, **20**(2), 95-102.

Yang, C.K. and Kim, M.H. (2011), "The structural safety assessment of a tie-down system on a tension leg platform during hurricane events", *Ocean Syst. Eng*., **1**(4), 263-283.

Zhang, Z., Kim, M.H. and Ward, E.G. (2009), "Progressive mooring-line failure of a deepwater MODU in hurricane conditions", *Proceedings of the 28th International Offshore Mechanics and Arctic Engineering Conference*, Honolulu.